Preservation of naïve phenotype CD4$^+$ T cells after vaccination contributes to durable immunity

Yi-Gen Pan[1], Laurent Bartolo[1], Ruozhang Xu[1, 2], Bijal Patel[1, 2], Veronika I. Zarnitsyna[3], Laura F. Su[1, 2*]

[1] Department of Medicine, Division of Rheumatology, Perelman School of Medicine, University of Pennsylvania, Philadelphia, PA 19104, USA.

[2] Corporal Michael J Crescenz VA Medical Center, Philadelphia, PA, 19104, USA.

[3] Department of Microbiology and Immunology, Emory University, Atlanta, GA, USA

Contact info

* Corresponding author and lead contact:

Laura F. Su

University of Pennsylvania

421 Curie Blvd BRBII/III 311

Philadelphia, PA 19104

215-898-4181

Laurasu@upenn.edu

Abstract

Memory T cells are conventionally associated with durable recall responses. In our longitudinal analyses of CD4$^+$ T cell responses to the yellow fever virus (YFV) vaccine by peptide-MHC tetramers, we unexpectedly found CD45RO$^-$CCR7$^+$ virus-specific CD4$^+$ T cells that expanded shortly after vaccination and persisted months to years after immunization. Further phenotypic analyses revealed the presence of stem-cell memory T cells (T_{SCM}) within this subset. In addition, post-vaccine T cells lacking known memory markers and functionally resembling genuine naïve T cells were identified, referred to herein as marker-negative T cells (T_{MN}). Single-cell TCR sequencing detected expanded clonotypes within the T_{MN} subset and identified T_{MN} TCRs shared with memory and effector T cells. Longitudinal tracking of YFV-specific responses over subsequent years revealed superior stability of T_{MN} cells, which correlated with the longevity of the overall tetramer$^+$ population. These findings uncovered additional complexity within the post-immune T cell compartment and implicate T_{MN} cells in durable immune responses.

Brief summary

Naïve phenotype CD4$^+$ T cells persist after vaccination. These cells may contribute to durable protective immunity.

Introduction

Functional immunological memory underlies the protective efficacy of vaccines against subsequent infections (1, 2). However, the reason why protection from some vaccines lasts decades while others wane after a few months remains unknown. A crucial aspect of immune memory involves CD4$^+$ T cells (3). CD4$^+$ T cells provide key signals for B cell maturation and high-affinity antibody production (4). They are also needed to support the expansion and maintenance of functional CD8$^+$ T cells and can directly contribute to anti-viral effects (4-6). Past studies in mice and humans have identified naïve-like antigen-experienced T cells with superior longevity and plasticity as a source of durable memory (7-9). Broadly categorized as stem cell-like memory T cells

(T_{SCM}), these cells phenotypically resemble naïve T cells by positive CCR7 and CD45RA or negative CD45RO expression, yet they display differentiation markers such as CD95, CXCR3, and CD49d (9-11). In people immunized with the highly efficacious and durable Yellow Fever Virus (YFV) vaccine, class I tetramer analyses identified T_{SCM} as the predominant phenotype of virus-specific $CD8^+$ T cells greater than 8 years after vaccination (10, 12).

The durability of $CD4^+$ T cell memory is less understood. Although capable of differentiating into T_{SCM} cells (13-16), $CD4^+$ T cells are generally less responsive to homeostatic cytokines IL-7 and IL-15 (17-19), which augment T_{SCM} differentiation in cultured $CD8^+$ T cells (20). Here, we examined virus-specific $CD4^+$ T cells after YFV vaccination to delineate key features of durable $CD4^+$ T cell responses. YFV-specific $CD4^+$ T cells were identified and tracked longitudinally by direct *ex vivo* class II peptide-MHC (pMHC) tetramers staining. We showed the presence of various memory subsets within YFV-specific $CD4^+$ T cells several months after vaccination, including T_{SCM} cells. Unexpectedly, about a quarter of $CD45RO^-CCR7^+$ tetramer-labeled T cells, lacked CD95, CXCR3, CD11a, and CD49d expression, distinguishing them from T_{SCM} cells. These marker negative T cells (T_{MN}) were a part of expanded clonotypes and shared TCR sequences with memory and effector T cells, suggesting *in vivo* antigen responses. T_{MN} cells showed minimal decay over years and correlated with the stability of $tetramer^+$ populations. Our findings expand the current definition of antigen-experienced T cells to include those that retained an undifferentiated phenotype. These T_{MN} cells may contribute to durable immunity.

Results

Detection of naïve-like $CD4^+$ T cells after YFV vaccination

We had previously performed a longitudinal study of YFV-specific $CD4^+$ T cells to evaluate the impact of pre-existing repertoire on T cell responses to primary immunization with the YFV vaccine (21). Starting with this dataset, we examined features of memory T cells that developed at least 7 months after vaccination. This showed that approximately half of the YFV-specific memory pool consisted of central memory T cells (T_{CM}), with about 21% of $tetramer^+$ cells retaining a naïve-like $CD45RO^-CCR7^+$ phenotype (Fig. 1A-B). Proportionally, the abundance of $CD45RO^-CCR7^+$ subset was highest before vaccination, decreased initially post-vaccination, then reaccumulated several months later (Fig. 1C). Quantified as cells per million $CD4^+$ T cells, $CD45RO^-CCR7^+$ $tetramer^+$ cells quickly increased and reached a peak approximately 1 month after vaccination (Fig. 1D). The frequency of $CD45RO^-CCR7^+$ T cell subset did not differ significantly by donor age and was associated with the robustness of the response (Fig. S1A-C). At the memory time point, $CD45RO^-CCR7^+$ YFV-specific T cells were more abundant in $tetramer^+$ populations that reached a higher frequency and correlated with efficient recruitment of memory cells (Fig. 1E-F). These data suggest that $CD45RO^-CCR7^+$ $CD4^+$ T cells is a feature of an effective T cell response.

Post-immune T cells are heterogeneous and include a differentiation marker negative subset

We hypothesized that the post-vaccine $CD45RO^-CCR7^+$ subset largely consisted of T_{SCM} cells as in $CD8^+$ T cells (10, 12). To test this, we performed tetramer staining on 28 YFV-specific $CD4^+$ populations from 7 individuals, recognizing 16 unique epitopes with antibodies against T_{SCM}-associated markers, CXCR3, CD95, CD11a, and CD49d (Tables S1 and S2). Staining with this broader antibody panel on blood collected 7 to 48 months after vaccination indeed identified $CD45RO^-CCR7^+$ $tetramer^+$ T cells that expressed one or more T_{SCM} markers. However, we noted that a portion of $CD45RO^-CCR7^+$ $CD4^+$ T cells remained negative for CXCR3, CD95, CD11a, and CD49d expression (Fig. 2A, S2A-D). To gain further insights into the heterogeneity within the CD45RO-$CCR7^+$ subset, we combined 1465 YFV-specific $CD4^+$ T cells from one donor and visualized combinatorial antibody staining on UMAP using the Spectre pipeline (22). This identified regions with low CD45RO and high CCR7 signals, which encompassed a $CXCR3^+$ (cluster 0) and a T_{SCM} marker negative population (cluster 4) (Fig. 2B-D). We defined $CD45RO^-CCR7^+$ cells lacking any measured differentiation markers as marker-negative T cells (T_{MN}) and classified those expressing at least one of CXCR3, CD95, CD11a, or CD49d as T_{SCM} cells (Table S3). We then performed manual gating and used Boolean combinations of these gated cells to subdivide $CD45RO^-CCR7^+$ subset into T_{MN} and various T_{SCM} combinations (Fig. S2B-D). On average, 27% of the $CD45RO^-CCR7^+$ subset consisted of T_{MN} cells (Fig. 2E). Among T_{SCM} cells, approximately a quarter expressed only one differentiation marker, with CXCR3 being the most common (Fig. 2E-F). Finding antigen-specific T cells that do not express known memory or T_{SCM} markers after a clear prior exposure was unexpected. To test if T_{MN} cells functionally behave like antigen-experienced T cells despite

lacking surface markers of differentiation, we treated post-vaccine PBMCs with PMA and ionomycin for 4 to 5 hours. Antigen-specific T cells were captured by tetramers, divided into distinct phenotypic subsets, and analyzed for TNF-α and IFN-γ production. This showed that post-immune T_{MN} subset produced significantly less cytokines compared to memory T cells within the same tetramer$^+$ population (Fig. 2G-H). Thus, YFV vaccination induced a diverse post-immune repertoire that included CD4$^+$ T_{SCM} cells and a naïve-like T_{MN} population that lacked phenotypic and functional features of antigen experience.

Virus-specific T_{MN} cells respond to antigens

We were intrigued by the existence of virus-specific T cells that retained a naïve functional phenotype after vaccination. Past studies have identified non-stimulatory TCR interactions that decoupled T cell activation from ligand binding (23). The impaired ability to respond productively to antigens may be one reason why some tetramer-labeled T cells retained a naïve phenotype. To investigate this possibility, we quantified T_{MN}, T_{SCM}, and T_{CM} cells for differences in their functional avidity by peptide stimulation. YFV-specific T cell clones were generated using samples from two donors obtained 7 to 8 months after YFV vaccination. Among the 48 clones that grew, 40 clones (90%) had the correct specificity by tetramer re-staining and/or response to peptides (Fig. 3A-B, S3A). We did not identify peptide-nonresponsive T cells as all clones that were stained with tetramers responded to peptide stimulation. To determine if T_{MN} cells might be harder to activate due to a lower functional avidity, we divided the clones according to their direct *ex vivo* phenotype and selected 5 clones each from T_{CM}, T_{SCM}, T_{MN} groups for further analyses. YFV-specific clones were stimulated with decreasing concentrations of the cognate peptide and analyzed for response by cytokine production (Fig. S3B). T_{MN}-derived clones responded similarly to peptides by TNF-α production, with no significant differences in maximal effective peptide concentration (EC50) values between groups (Fig. 3C-D). T cell clones, regardless of their *ex vivo* phenotypes, also produced similar levels of IFN-γ, IL-2, and had comparable TNF-α^+IFN-γ^+IL-2$^+$ co-expression (Fig. 3E). In addition, we evaluated the proliferative capacity of T_{MN}, T_{SCM}, and T_{CM}-derived clones by CellTrace Violet (CTV) dilution and observed no significant differences in the proliferative response to peptide stimulation (Fig. 3F-G, Fig. S3C). Thus, TCR-ligand engagement is likely intact for vaccine-specific T cells that retained a naïve phenotype after vaccination.

Antigen-experienced T_{MN} cells

While T_{MN} cells respond well to antigens *in vitro*, it remains possible for them to be less competitive in resource-limiting environments. To investigate this, we reason that we can use TCR sequences to infer stimulation and proliferative response *in vivo*. Because T cell progenies originating from a T cell express identical TCR sequences, we can further leverage these sequences as molecular barcodes to investigate the clonal relationship between distinct phenotypic subsets. However, capturing sufficient numbers of T_{MN} cells was challenging due to their limited number within the available blood samples. To overcome this problem, we generated new tetramers using affinity-matured HLA-DR monomers containing mutations that enhanced CD4 binding to improve the overall capture efficiency (24). When compared to the wild-type (wt) DR, these tetramers stained a larger population of T cells without significantly skewing the phenotypic proportions (Fig. S4A-C). In total, we sorted single cells from 5 tetramer-labeled populations and obtained TCR sequences from 607 YFV-specific CD4$^+$ T cells after amplification and sequencing (Fig. 4A, Table S4). Consistent with clonal expansion after vaccination, over 70% of the sequences were identified in multiple tetramer-sorted T cells. Among expanded sequences, 25 to 52% were abundant and found in at least 10 individual T cells (Fig. 4B). Most T cells displayed a T_{CM} or T_{EM} phenotype based on antibody staining at the time of sorting. T_{MN} phenotype was infrequent, expressed by 3 to 4% of sequenced T cells and confined to the two most extensively sequenced populations recognizing YF45. Consistent with *in vivo* expansion, T_{MN} cells did not preferentially express unique TCRs, but rather, they were distributed across various clone sizes (Fig. 4C). We focused the subsequent analyses on YF45-specific T cells that included the T_{MN} subset. Early post-vaccine measurements of YF45-specific T cells from HD2 and HD3 showed that both populations had generated robust responses to the YFV vaccine (Fig. 4D) (21). In agreement with an antigen-driven response, T_{MN} cells contained expanded clonotypes and shared overlapping sequences with various memory subsets (Fig. 4E-F, S4E). In separately generated T cell clones from the same individuals, T_{MN}-derived clones expressed TCRs that matched the sequences from *ex vivo* sorted T cells of diverse clone sizes and phenotypes (Fig. S4F).

The presence of shared TCR sequences with memory T cells, together with clonal expansion, suggest that T_{MN} cells had encountered and responded to antigens. Alternatively, clonotype sharing between memory and naïve cells may be explained by the presence of multiple naïve T cells with the same TCR, where a portion did not

encounter YFV antigen and remained naïve. To investigate this possibility, we examined the pre-vaccination repertoire of YF45-specific T cells in these individuals to determine if pre-exposure T cells expressing T_{MN}-associated TCRs were abundant before vaccination (21). The changes in clonal dynamics were assessed by tetramer staining, sorting, and sequencing the TCRs of YF45-specific T cells from blood collected 14 days after vaccination. Of note, the sampling depth at day 14 was much shallower due to limited sample availability. Ten to twenty million PBMCs was used for tetramer staining versus over a hundred million $CD4^+$ T cells were used to capture rare precursor T cells in the pre-vaccine sample. In total, we examined TCR sequences from 129 precursor T cells and 238 effector T cells (Fig. 5A, Table S5). Before vaccination, no pre-vaccine TCRs matched T_{MN}-derived TCRs from HD2 and only one sequence was identified in HD3. This shared TCR mapped to a unique sequence and not to the expanded pre-existing clonotypes in this individual (Fig. 5B-C). Fourteen days following vaccination, matched TCR frequencies increased to 7% in HD2 and 23% in HD3, capturing a total of 7 clonotypes (Fig. 5B-C). The majority of matched clonotypes were expanded and expressed by a variety of differentiated cells (Fig. 5D). Among T cells without a T_{MN} match, two cells in HD3 were T_{MN}-like and lacked differentiation marker expression. One of these cells was found as a part of an expanded clone at day 14 and shared the same TCR with multiple memory T cells in the day 210 sample (Fig. 5E, Table S5). Additionally, the post-vaccine day 14 blood from this donor contained three $CD45RO^-CCR7^+$ T cells without additional differentiation marker staining (Table S5).

Human T cells stimulated with cytokines can maintain a naïve phenotype (25). Our data suggest that this can also occur with antigen-specific responses. To broaden the analyses, we compared the frequency of $CD45RO^-CCR7^+$ T cells in various YFV-specific populations before and after YFV vaccination (Fig. 5F). This showed an increase in $CD45RO^-CCR7^+$ $tetramer^+$ cells post-exposure, which included diverse ratios of T_{SCM} and T_{MN} cells (Fig. 5G). We focused on the T_{MN} subset as they resembled unstimulated naïve T cells. If there is no mechanism to replenish the naïve repertoire and/or hold on to a naïve phenotype, we expected a decrease in naïve cell frequency following an immune response as responding T cells acquire differentiated states. However, contrary to this, the averaged post-vaccine T_{MN} cell frequency was comparable to the frequency of naive cells before vaccination (Fig. 5H). To examine population-level differences, we divided post-vaccine T_{MN} frequency of each population by its initial naïve T cells frequency before vaccination. This revealed lower T_{MN} frequencies in two-third of the populations, while the remaining third showed an increase (Fig. 5I). The absence of a reduction in naïve T cells did not indicate a lack of responsiveness to the vaccine. Instead, among the ten populations that gained naive T cells, there was a higher averaged fold-change in total $tetramer^+$ frequency before and after vaccination (Fig. 5J). Collectively, these data suggest T_{MN} subset comprises T cells that had responded to vaccination.

T_{MN} cells contribute to durable memory

While memory T cells are essential for generating rapid recall responses, naïve T cells are known for their long life-span and regenerative potential (26, 27). Therefore, we hypothesized that T_{MN} cells promote the durability of antigen-specific responses after vaccination. To test this idea, we analyzed additional time points from five donors with longitudinal PBMCs collected up to 6.7 years after YFV vaccination (Fig. 6A, Fig. S5A). Past modeling of cellular turnover suggests that different phenotypic subpopulations undergo separate and distinct *in vivo* dynamics (28, 29). To evaluate the stability of individual phenotypic subsets, we subdivided 19 YFV-specific populations according to T_{MN}, T_{SCM}, T_{CM}, T_{EM}, and T_{EMRA} phenotypes based on CD45RO, CCR7, CD95, CXCR3, CD11a, and CD49d expression. Their time-dependent change was quantified as a fitted slope using a mixed-effects exponential decay model. This revealed different rates of decay between cells in distinct differentiation states. $CD4^+$ T_{EM} cells had the largest negative slope, indicating the greatest decrease over time. In contrast, T_{MN} cells exhibited remarkable stability, with no discernible decline observed during the follow-up period. The stability of the T_{MN} subset significantly surpassed that of other phenotypic subsets, including T_{SCM} and T_{CM} cells, which are typically considered to be long-lived (Fig.6B).

Next, we examined the decay kinetics of the overall $tetramer^+$ populations. Because some data were generated before switching to modified DR, paired analyses by wildtype and modified tetramers on the same blood sample were used to generate an equation for normalizing the frequencies across experiments (Fig. S4D). Among the five donors followed longitudinally, two received one YFV dose as typical for the YFV vaccine, while three received a second YFV vaccine 7 months to a year after the initial dose (Table S6). Re-vaccination was originally a part of an IRB-approved protocol to study recall response. While this strategy did not effectively induce acute T cell responses, likely due to YFV neutralization by antibodies generated from the

first vaccination, we investigated whether it might still impact long-term T cell dynamics. We divided tetramer$^+$ populations based on donors' vaccine doses. Consistent with the longevity of YFV vaccine-mediated protection, YFV-specific CD4$^+$ T cells displayed an average half-life ($t_{1/2}$) of close to 4 years after one YFV immunization (Fig. 6C). This durable response was further stabilized after re-exposure in the two-dose group (Fig. S5B).

T_{MN} cell frequencies did not significantly differ between the one-dose and two-dose groups (Fig. S5C). Given the wide variation in T_{MN} cells, we divided tetramer$^+$ populations based on T_{MN} frequency into top and bottom halves (Fig. 6D). This showed that populations with more T_{MN} cells were more stable compared to populations in the bottom T_{MN} group (Fig. 6E). The T_{MN} frequency within a given virus-specific population further positively correlated with the stability of the overall population (Fig. 6F). By contrast, we did not find significant differences between high and low groups based on T_{SCM}, T_{CM}, T_{EM}, and T_{EMRA} frequencies (Fig. S5D). On the phenotypic level, all tetramer$^+$ populations contained various memory subsets, but the top T_{MN} group was more phenotypically diverse. We divided populations based on the first T_{MN} frequency obtained within the 1-2 years after YFV vaccination and showed that populations with more T_{MN} cells exhibited greater diversity of differentiation states over time as measured by the Shannon diversity index (Fig. 6G-H). Collectively, these data highlight the stability of the T_{MN} subset and uncover their association with durable and diverse T cell memory after YFV vaccination.

Discussion

A T cell is typically referred to as naïve if it has not yet encountered its specific cognate antigen(s). However, a clear antigenic history is often not available in human studies, and thus specific surface markers are commonly used to infer antigen experience (11, 30). Here, we examined CD4$^+$ T cell memory to YFV vaccination to define key features of durable memory by direct *ex vivo* class II tetramer staining and enrichment. This showed a diverse memory pool comprised of various differentiation states after YFV vaccination. Surprisingly, we also uncovered an increase in naïve phenotype YFV-specific T cells after vaccination.

Deeper phenotypic analyses showed that a portion of CD45RO$^-$CCR7$^+$ cells was previously described T_{SCM} cells. The remaining cells did not express known surface markers of T cell differentiation that were tested. We evaluated several potential explanations for their origin. Our initial idea that T_{MN} cells were unresponsive was incorrect. Peptide-stimulated T_{MN}-derived T cell clones produced robust levels of cytokines at comparable EC50 as T cell clones generated from memory cells. The presence of expanded TCR clones within the T_{MN} subset further suggest that some T_{MN} cells had seen and responded to antigens *in vivo*. The observation that T_{MN} cells, memory, and effector T cells have overlapping TCR repertoires suggests shared precursors among these subsets and provide additional support to the idea that some T_{MN} cells are antigen-experienced as their common precursors divided at least once in response to antigen. This extent of overlap would not be expected if clonal expansion within T_{MN} subset were driven by different processes, such as cytokine-mediated and/or bystander response. Our interpretation that some expanded antigen-experienced cells exist within the T_{MN} population is further supported by increased naïve T cell frequency following immunization. We show that, despite recruitment into effector responses, the frequency of naïve T cell frequency recognizing YFV is largely unchanged. Among populations analyzed pre- and post-immunization, approximately a third gained more naïve phenotype T cells in the form of T_{MN} cells above their pre-vaccine baseline. Probabilistically, it is also unlikely to capture T_{MN} cells 14 days after vaccination if they had not expanded, since the same clonotype was not detected before vaccination despite analyzing many more cells.

In addition to an antigen-experienced subset, some T_{MN} cells could be genuine naïve T cells. As an alternative possibility, there might be multiple naïve cells of the same clonotype but only a subset responded to the vaccine. Incomplete response may have occurred because some YFV-specific T cells were not at the right place or time to respond to the immunogen. Other cells may not have received enough of the appropriate signal to undergo expansion and/or differentiation (33). This model could be consistent with our TCR data but does not explain why certain specificities contain higher frequencies of naïve T cells after vaccination. An intriguing alternative for this increase might involve ongoing thymic activities. Although thymic output for new T cells declines with age, recent thymic emigrants remain detectable in adults (34-36). Newly produced T cells might add to the peripheral T_{MN} pool to increase the abundance of YFV-specific naïve T cells after vaccination. T_{MN} cells from various sources could contribute to the naïve repertoire after antigen exposures, varying in their impact depending on antigen-specificity, the type of stimulation, age and other individual characteristics.

Only a few select vaccines are capable of mediating life-long protection. How durable immunological memory is maintained remains a key unresolved question. While Memory T cells are the cornerstone of protective immunity by virtue of their ability to rapidly initiate a functional response to pathogen rechallenge, naïve T cells possess superior self-renewal capacity and differentiation plasticity (3, 26, 37). Irrespective of how T_{MN} cells might have originated, we asked whether T_{MN} cells are related to the longevity of T cell response. Our findings revealed remarkable stability of the T_{MN} population, showing minimal decay for nearly 7 years. These stable T cells could potentially support the longevity of the overall immune response, extending it beyond the lifespan of individual memory T cells. Consistent with this model, T_{MN} cells are more abundant in durable $CD4^+$ populations that are stable over time. Based on the diverse memory phenotypes in T_{MN}-enriched populations, we further speculate that T_{MN} cells have the potential to differentiate into multiple states, thereby contributing to the phenotypic diversity of T cell memory.

In summary, our findings highlight the complexity within the post-immune T cell compartment and add to our understanding of the diverse spectrum of T cells exhibiting naïve features (27, 38). Using an antigen-specific approach, our data suggest that some cells considered naïve by phenotypic criteria are actually antigen-experienced. As a whole, post-immune T_{MN} cells are remarkably stable. Understanding how T_{MN} cells are generated, maintained, and work alongside memory cells in providing long-lasting immune protection could aid the future development of improved vaccine strategies.

Limitation of study

We did not further subset T_{MN} cells to evaluate potential heterogeneity in gene-expression, epigenetic landscape, or functional attributes due to the limitations on cell numbers. Future studies using models allowing manipulation of T_{MN} cells will be needed to build on their association with durable immunity and establish causation. As our analyses are focused on $CD4^+$ T cell responses to YFV in a few healthy individuals, larger studies involving additional vaccines will be important to strengthen our findings and to understand how the T_{MN} subset influences vaccine durability across different age and disease settings.

Acknowledgments: We thank our study subjects for their participation.

Funding: NIH R01AI134879 (L.F.S), NIH R01AI66358 (L.F.S), VA Merit Award I01CX001460(L.F.S), VA COVID Award I01BX005422 (L.F.S), CHU fund (L.F.S)

Author contributions: Conceptualization, L.F.S.; Experimentation, Y.P.; Sequence analyses, L.B.; High-dimensional phenotypic analyses, R.X.; Study recruitment, B.P; Modeling and statistical support, V.Z.; Supervision, L.F.S.; Manuscript preparation, L.F.S., V.Z, L.B., and Y.P.

Competing interests: The authors declare no competing interests.

Methods

Sex as a biological variable

Both male and female participants were included in this study. Study volunteers were recruited in the order of participation without restrictions based on the sex.

Human samples

This study uses cryopreserved cells stored in fetal bovine serum (FBS) with 10% DMSO from an ongoing vaccine study at the University of Pennsylvania (21). This study includes 7 healthy adult participants with no prior YFV exposure who received one or two doses of the 17D live-attenuated YFV vaccine (YF-VAX®, Sanofi Pasteur). Individuals older than 65 were excluded. As YFV vaccine provides life-long protection against YFV, re-vaccination with the attenuated 17D-204 strain is not expected to increase risk. Five participants were followed longitudinally for 2 to 6.7 years after vaccination. All samples were de-identified and obtained with IRB regulatory approval from the University of Pennsylvania. Subject characteristics are shown in Table S1.

Cell lines

Hi5 cells (ThermoFisher) were maintained by insect cell culture medium (ESF921, Expression Systems) supplemented with 0.02% gentamicin at 28°C.

Protein expression and tetramer production

HIS-tagged HLA-DRA/B1*0301, 0401, 0407, and 1501 protein monomers of wild type (wt) sequence or with L112W, S118H, V143M, T157I mutations (24) were produced by Hi5 insect cells and extracted from culture supernatant using Ni-NTA (Qiagen). HLA-DR monomers were biotinylated overnight at 4°C using BirA biotin ligase (Avidity) and purified by size exclusion chromatography using Superdex 200 size exclusion column (AKTA, GE Healthcare). Biotinylation was confirmed by gel-shift assay. Peptide exchange and tetramerization for wildtype and modified affinity-matured DR were performed using standard protocols as previously described (39, 40). In brief, HLA-DR proteins were incubated with thrombin (Millipore) at room temperature for 3 - 4 hours and exchanged with peptides of interest in 50-fold excess at 37°C for 16 hours. Peptide-loaded HLA-DR monomers were incubated with fluorochrome-conjugated streptavidin at 4 - 5: 1 ratio for 2 min at room temperature, followed by a 15 min incubation with an equal volume of biotin-agarose slurry (Millipore). Tetramers were buffered exchanged into PBS, concentrated using Amicon ULTRA 0.5ml 100KDa (Millipore), and kept at 4 °C for no more than 2 weeks prior to use.

***Ex vivo* T cell analyses and cell sorting**

Phenotypic analyses and frequency quantification: Tetramer staining was performed on at least 10 million PBMCs with 5 ug of tetramers in 100 μl reaction for 1 hour at room temperature as previously described (21, 40, 41). Tetramer-tagged cells were enriched by adding anti-fluorochrome and anti-HIS MicroBeads (MiltenyiBiotec). The mixture was passed through LS columns (MiltenyiBiotec). Column-bound cells were washed and eluted according to manufacturer protocol. For antibody staining, the enriched samples were stained with viability dyes and exclusion markers (anti-CD19 and anti-CD11b, Table S7), along with combinations of surface markers as specified in the experiments (anti-CD3, anti-CD4, anti-CD45RO, anti-CCR7, anti-CD11a, anti-CD95, anti-CD49d, and anti-CXCR3, Table S7), in 50 to 100ul of FACS buffer (PBS plus 2% FCS, 2.5mM EDTA, 0.025% Sodium Azide) for 30 minutes at 4°C. Samples were fixed with 2% paraformaldehyde and acquired by flow cytometry using LSRII (BD). Data analyses were performed by FlowJo (BD). The Boolean tools was used to define T_{SCM} and T_{MN} cells within the $CD45RO^{-}CCR7^{+}$ subset. Frequency calculation was obtained by mixing 1/10th of samples with 200,000 fluorescent beads (Spherotech) for normalization.

For longitudinal experiments involving both wt and modified DR, paired data from wt and modified DR, with a minimum of two data points per time point for each specificity, were used to derive the equation for normalization: $\log_2(Freq_{modified})=3.72+0.35 * \log_2(Freq_{wt})$ (Fig. S4D). Frequencies generated by wt tetramers that were below the normalized values were adjusted. Mixed effects exponential decay models were used to analyze longitudinal changes in antigen-specific T cell populations and estimate the corresponding slopes. These models were implemented in *MonolixSuite 2021R1* (Lixoft) and fitted to data after vaccination. Initial T cell specificity values were lognormally distributed, exponential decay rates were normally distributed, and lognormal multiplicative error was used. The estimation of the population parameters was performed using the Stochastic Approximation Expectation-Maximization (SAEM) algorithm. Half-lives were calculated as ln(2)/*k*, where the corresponding *k* values represented the estimated exponential decay rate constants. Estimated decay rates were converted into slopes as -*k*.

For multi-dimensional analyses, a total of 1465 manually gated $tetramer^{+}$ cells were exported from FlowJo, read into R by flowCore, and combined into one single dataset for subsequent data processing and analyses using the Spectre package in R (22). Staining intensities were converted using Arcsinh transformation with a cofactor of 200. Batch alignment was performed using the CytoNorm (42). Clustering was performed using Phenograph with nearest neighbors set to 55 (k = 55) (43). UMAP was used for dimensional reduction and visualization (44).

Function response: T cells were rested overnight, followed by 4 - 5 hours of stimulation by phorbol myristate acetate (PMA, 5 ng/ml, Sigma) and ionomycin (500 ng/ml, Sigma) in the presence of monensin (2 uM, Sigma) and Brefeldin A (5 ug/ml, Sigma). Tetramer and surface antibody staining were performed as above. Intracellular staining with antibodies to TNF-α, IFN-γ, CD3 and CD4 (Table S7) was performed following BD Cytofix/Cytoperm Fixation/Permeabilization Kit according to manufacturer protocol (BD).

Cell sorting: Around 60 million $CD3^+$ or $CD4^+$ T cells were used and stained with up to 10 ug of each tetramer in a 100 ul reaction. Antibody staining was performed as above without fixation. Individual tetramer-labeled cells were isolated for TCR sequencing or T cell cloning by index sorting using the purity mode on FACS Aria (BD).

Generation and stimulation of T cell clones

Clone generation: Cells were stained with tetramers and enriched with magnetic beads as described above. Single tetramer-stained $CD4^+$ T cells were sorted into individual wells in a round bottom 96-well plate containing 10^5 irradiated PBMCs, 10^4 JY cell line (ThermoFisher), PHA (1:100, ThermoFisher), IL-7 (25 ng/ml, PeproTech), and IL-15 (25 ng/ml, PeproTech). IL-2 (50 IU/ml, PeproTech) was added on day 5 and replenished every 3-5 days. Cells were resupplied with fresh medium with IL-2 (50 IU/ml), PHA (1:100), and 10^5 irradiated PBMCs every two weeks.

DCs generation: Monocytes from HLA-DR allele-matched donors were isolated using negative enrichment kits (RosetteSep Human Monocyte Enrichment Cocktail, StemCell). 10 million cryopreserved monocytes were cultured in 15 ml DC media (RPMI 1640 plus Glutamine,10% FCS, 1X Pen/Strep, 10 mM HEPES) in the presence of 100 ng/ml GM-CSF and 500 U/ml IL-4. Three days later, half the culture media was replaced with fresh DC media with 100 ng/ml GM-CSF, 500 U/ml IL-4, and 0.05 mM 2-mercaptoethanol. Cells in suspension were harvested at 5 to 6 days and added to a flat-bottom 96-well plate at 25,000 DCs per well. DCs were treated with 100 ng LPS and peptides (0.00001 ug/ml to 10ug/ml) for 16 hours and replenished with fresh media before co-culturing with T cells.

Stimulation of T cell clones: T cell clones were rested overnight in fresh media without IL-2 and added to wells containing matured DCs at 1:1 ratio in the presence of monensin (2 uM, Sigma) and Brefeldin A (5 ug/ml, Sigma). After 5 hours, cells were transferred into a new 96-well round bottom plate, washed once with FACS buffer, and stained with viability dyes, exclusion markers (anti-CD19 and anti-CD11b) for 30 minutes at 4°C. Intracellular staining with antibodies to TNF-α, IFN-γ, IL-2, CD3 and CD4 (Table S7) was performed following BD Cytofix/Cytoperm Fixation/Permeabilization Kit according to manufacturer protocol (BD). Half maximal effective concentration (EC50) was determined using the percentage of T cell clones that produced TNF-α in response to decreasing peptide concentrations (10, 1, 0.1, 0.01, 0.001, 0.0001, and 0.00001 ug/ml). A non-linear fit without constraint was applied to log-transformed concentration using the equation Y=Bottom + (Top-Bottom)/(1+10^((LogEC50-X)*HillSlope)) in Prism (GraphPad). For proliferation assay, T cell clones were labeled with 1:1000 diluted CellTrace Violet (CTV, ThermoFisher Scientific) following manufacturer protocol. The CTV-stained cells were rested in fresh media without IL-2 for 16 hours. 25,000 rested T cells were co-cultured with DC pulsed with 10 ug/ml cognate peptides or treated with PHA as a positive control (1:100, ThermoFisher). After 5 days, cells were harvested and stained with viability dyes and surface antibodies (anti-CD19, anti-CD11b, anti-CD3, and anti-CD4 for 30 minutes at 4°C followed by fixation with 2% paraformaldehyde. Samples were acquired by flow cytometry using LSRII (BD) and analyzed by FlowJo (BD).

Single-cell TCR sequencing and analyses

Single-cell TCR Sequencing by nested PCRs was performed using the primer sets and the protocol as previously described (21, 45). In brief, reverse transcription was performed with CellsDirect One-Step qRT-PCR kit according to the manufacturer's instructions (CellsDirect, Invitrogen) using a pool of 5' TRVB-region specific primers and 3' C-region primers. The cDNA library was amplified using a second set of multiple internally nested V-region and C-region primers with HotStarTaq DNA polymerase kit (Qiagen). The final PCR reaction was performed on an aliquot of the second reaction using a primer containing common base sequence and a third internally nested Cβ primer. PCR products were gel purified (Qiagen) and sequenced on Novaseq 6000 platform (Illumina). TCR sequences were pre-processed as previously described (21). In brief, forward and reverse reads were converted into one paired end read using pandaseq (46). Data were demultiplexed by the unique combination of plate, row, and column barcodes. Consensus TCRβ sequences were identified using the V(D)J alignment software MiXCR (47). A threshold of a read count of 200 reads per sequence was applied to the consensus sequences. If more than one TCRα or TCRβ chain passes this criterion we retain the dominant TCRβ and the two TCRα chains with the highest read count. For data obtained from cells several months after vaccination, we additionally require phenotypic annotation based on antibody staining from index sort data. Data were excluded if phenotypic information was not retained or ambiguous. For

downstream analyses, data wrangling was performed using the tidyverse package. TCRs were matched by TCRβ if only the beta chain was available, or by TCRβ plus at least one TCRα if alpha chain(s) were called. Circos plots were made using the circlize package of R software (48).

Statistics

Normality was assessed using D'Agostino-Pearson test. Spearman was used if either of the two variables being correlated was non-normal. Otherwise, Pearson was used to measure the degree of association. Least squares linear regression was used to calculate the best-fitting line. Statistical comparisons were performed using two-tailed Student's t-test, paired t-test, Welch's one-way ANOVA, repeated measures one-way ANOVA, two-way ANOVA, or mixed effects model. A p-values of <0.05 was used as the significance level and adjusted if multiple comparisons were performed. Statistical analyses were performed using GraphPad Prism. Lines and bars represent the mean and variability is represented by the standard error of the mean (SEM). * $P < 0.05$, ** $P < 0.01$, *** $P < 0.001$, **** $P < 0.0001$.

Study approval

All participants have given written informed consent. The study was approved by the Institutional Review Board at the University of Pennsylvania, Philadelphia (approval 820884).

Data availability

All data needed to evaluate the conclusions in the paper are present in the paper or the supplementary materials. Analyses are performed using standard analysis packages. All data points are reported in the Supporting Data Values file. Further information is available from the corresponding author on request.

References

1. Kathryn AF, Jason MS, Stephen CJ, Vaiva V, and David M. Preexisting high frequencies of memory CD8+ T cells favor rapid memory differentiation and preservation of proliferative potential upon boosting. *Immunity.* 2013;39(1):171-83.
2. Martin JR, Jeffrey CN, and John TH. Pathogen-Specific Inflammatory Milieux Tune the Antigen Sensitivity of CD8(+) T Cells by Enhancing T Cell Receptor Signaling. *Immunity.* 2012.
3. Wherry EJ, and Barouch DH. T cell immunity to COVID-19 vaccines. *Science.* 2022;377(6608):821-2.
4. Crotty S. T follicular helper cell differentiation, function, and roles in disease. *Immunity.* 2014;41(4):529-42.
5. Laidlaw BJ, Craft JE, and Kaech SM. The multifaceted role of CD4(+) T cells in CD8(+) T cell memory. *Nat Rev Immunol.* 2016;16(2):102-11.
6. Swain SL, McKinstry KK, and Strutt TM. Expanding roles for CD4(+) T cells in immunity to viruses. *Nat Rev Immunol.* 2012;12(2):136-48.
7. Gattinoni L, Lugli E, Ji Y, Pos Z, Paulos CM, Quigley MF, et al. A human memory T cell subset with stem cell-like properties. *Nat Med.* 2011;17(10):1290-7.
8. Zhang Y, Joe G, Hexner E, Zhu J, and Emerson SG. Host-reactive CD8+ memory stem cells in graft-versus-host disease. *Nat Med.* 2005;11(12):1299-305.
9. Pulko V, Davies JS, Martinez C, Lanteri MC, Busch MP, Diamond MS, et al. Human memory T cells with a naive phenotype accumulate with aging and respond to persistent viruses. *Nat Immunol.* 2016;17(8):966-75.
10. Fuertes Marraco SA, Soneson C, Cagnon L, Gannon PO, Allard M, Abed Maillard S, et al. Long-lasting stem cell-like memory CD8+ T cells with a naive-like profile upon yellow fever vaccination. *Science translational medicine.* 2015;7(282):282ra48.
11. Caccamo N, Joosten SA, Ottenhoff THM, and Dieli F. Atypical Human Effector/Memory CD4(+) T Cells With a Naive-Like Phenotype. *Frontiers in immunology.* 2018;9:2832.
12. Akondy RS, Fitch M, Edupuganti S, Yang S, Kissick HT, Li KW, et al. Origin and differentiation of human memory CD8 T cells after vaccination. *Nature.* 2017;552(7685):362-7.
13. Long HM, Chagoury OL, Leese AM, Ryan GB, James E, Morton LT, et al. MHC II tetramers visualize human CD4+ T cell responses to Epstein-Barr virus infection and demonstrate atypical kinetics of the nuclear antigen EBNA1 response. *J Exp Med.* 2013;210(5):933-49.

14. Buzon MJ, Sun H, Li C, Shaw A, Seiss K, Ouyang Z, et al. HIV-1 persistence in CD4+ T cells with stem cell-like properties. *Nat Med.* 2014;20(2):139-42.
15. Mpande CAM, Dintwe OB, Musvosvi M, Mabwe S, Bilek N, Hatherill M, et al. Functional, Antigen-Specific Stem Cell Memory (T(SCM)) CD4(+) T Cells Are Induced by Human Mycobacterium tuberculosis Infection. *Frontiers in immunology.* 2018;9:324.
16. Pawel M, Zachary AB, Sid PK, Christopher AK, Yun J, Luis S-P, et al. Th17 cells are long lived and retain a stem cell-like molecular signature. *Immunity.* 2011;35(6):972-85.
17. Tan JT, Ernst B, Kieper WC, LeRoy E, Sprent J, and Surh CD. Interleukin (IL)-15 and IL-7 jointly regulate homeostatic proliferation of memory phenotype CD8+ cells but are not required for memory phenotype CD4+ cells. *J Exp Med.* 2002;195(12):1523-32.
18. Cho JH, Kim HO, Surh CD, and Sprent J. T cell receptor-dependent regulation of lipid rafts controls naive CD8+ T cell homeostasis. *Immunity.* 2010;32(2):214-26.
19. Guimond M, Veenstra RG, Grindler DJ, Zhang H, Cui Y, Murphy RD, et al. Interleukin 7 signaling in dendritic cells regulates the homeostatic proliferation and niche size of CD4+ T cells. *Nat Immunol.* 2009;10(2):149-57.
20. Cieri N, Camisa B, Cocchiarella F, Forcato M, Oliveira G, Provasi E, et al. IL-7 and IL-15 instruct the generation of human memory stem T cells from naive precursors. *Blood.* 2013;121(4):573-84.
21. Pan YG, Aiamkitsumrit B, Bartolo L, Wang Y, Lavery C, Marc A, et al. Vaccination reshapes the virus-specific T cell repertoire in unexposed adults. *Immunity.* 2021.
22. Ashhurst TM, Marsh-Wakefield F, Putri GH, Spiteri AG, Shinko D, Read MN, et al. Integration, exploration, and analysis of high-dimensional single-cell cytometry data using Spectre. *Cytometry A.* 2022;101(3):237-53.
23. Sibener LV, Fernandes RA, Kolawole EM, Carbone CB, Liu F, McAffee D, et al. Isolation of a Structural Mechanism for Uncoupling T Cell Receptor Signaling from Peptide-MHC Binding. *Cell.* 2018;174(3):672-87 e27.
24. Sugata K, Matsunaga Y, Yamashita Y, Nakatsugawa M, Guo T, Halabelian L, et al. Affinity-matured HLA class II dimers for robust staining of antigen-specific CD4(+) T cells. *Nat Biotechnol.* 2021;39(8):958-67.
25. Soares MV, Borthwick NJ, Maini MK, Janossy G, Salmon M, and Akbar AN. IL-7-dependent extrathymic expansion of CD45RA+ T cells enables preservation of a naive repertoire. *J Immunol.* 1998;161(11):5909-17.
26. Gattinoni L, Speiser DE, Lichterfeld M, and Bonini C. T memory stem cells in health and disease. *Nat Med.* 2017;23(1):18-27.
27. van den Broek T, Borghans JAM, and van Wijk F. The full spectrum of human naive T cells. *Nat Rev Immunol.* 2018;18(6):363-73.
28. Asquith B, Debacq C, Macallan DC, Willems L, and Bangham CR. Lymphocyte kinetics: the interpretation of labelling data. *Trends Immunol.* 2002;23(12):596-601.
29. Gossel G, Hogan T, Cownden D, Seddon B, and Yates AJ. Memory CD4 T cell subsets are kinetically heterogeneous and replenished from naive T cells at high levels. *eLife.* 2017;6.
30. Mahnke YD, Brodie TM, Sallusto F, Roederer M, and Lugli E. The who's who of T-cell differentiation: human memory T-cell subsets. *Eur J Immunol.* 2013;43(11):2797-809.
31. Johannisson A, and Festin R. Phenotype transition of CD4+ T cells from CD45RA to CD45R0 is accompanied by cell activation and proliferation. *Cytometry.* 1995;19(4):343-52.
32. Qi Q, Liu Y, Cheng Y, Glanville J, Zhang D, Lee JY, et al. Diversity and clonal selection in the human T-cell repertoire. *Proc Natl Acad Sci U S A.* 2014;111(36):13139-44.
33. Evavold BD, and Allen PM. Separation of IL-4 production from Th cell proliferation by an altered T cell receptor ligand. *Science.* 1991;252(5010):1308-10.
34. den Braber I, Mugwagwa T, Vrisekoop N, Westera L, Mogling R, de Boer AB, et al. Maintenance of peripheral naive T cells is sustained by thymus output in mice but not humans. *Immunity.* 2012;36(2):288-97.
35. Junge S, Kloeckener-Gruissem B, Zufferey R, Keisker A, Salgo B, Fauchere JC, et al. Correlation between recent thymic emigrants and CD31+ (PECAM-1) CD4+ T cells in normal individuals during aging and in lymphopenic children. *Eur J Immunol.* 2007;37(11):3270-80.
36. Ryan DK, Tammy R, Lance EH, Patricia H, Mary Ann H, Roger D, et al. Homeostasis of the naive CD4+ T cell compartment during aging. *J Immunol.* 2008;180(3):1499-507.
37. Kunzli M, and Masopust D. CD4(+) T cell memory. *Nat Immunol.* 2023;24(6):903-14.

38. Thomson Z, He Z, Swanson E, Henderson K, Phalen C, Zaim SR, et al. Trimodal single-cell profiling reveals a novel pediatric CD8alphaalpha(+) T cell subset and broad age-related molecular reprogramming across the T cell compartment. *Nat Immunol.* 2023;24(11):1947-59.
39. Day CL, Seth NP, Lucas M, Appel H, Gauthier L, Lauer GM, et al. Ex vivo analysis of human memory CD4 T cells specific for hepatitis C virus using MHC class II tetramers. *J Clin Invest.* 2003;112(6):831-42.
40. Su LF, Kidd BA, Han A, Kotzin JJ, and Davis MM. Virus-Specific CD4(+) Memory-Phenotype T Cells Are Abundant in Unexposed Adults. *Immunity.* 2013;38(2):373-83.
41. Bartolo L, Afroz S, Pan YG, Xu R, Williams L, Lin CF, et al. SARS-CoV-2-specific T cells in unexposed adults display broad trafficking potential and cross-react with commensal antigens. *Sci Immunol.* 2022:eabn3127.
42. Van Gassen S, Gaudilliere B, Angst MS, Saeys Y, and Aghaeepour N. CytoNorm: A Normalization Algorithm for Cytometry Data. *Cytometry A.* 2020;97(3):268-78.
43. Levine JH, Simonds EF, Bendall SC, Davis KL, Amir el AD, Tadmor MD, et al. Data-Driven Phenotypic Dissection of AML Reveals Progenitor-like Cells that Correlate with Prognosis. *Cell.* 2015;162(1):184-97.
44. Becht E, McInnes L, Healy J, Dutertre CA, Kwok IWH, Ng LG, et al. Dimensionality reduction for visualizing single-cell data using UMAP. *Nat Biotechnol.* 2018.
45. Han A, Glanville J, Hansmann L, and Davis MM. Linking T-cell receptor sequence to functional phenotype at the single-cell level. *Nat Biotechnol.* 2014;32(7):684-92.
46. Masella AP, Bartram AK, Truszkowski JM, Brown DG, and Neufeld JD. PANDAseq: paired-end assembler for illumina sequences. *BMC bioinformatics.* 2012;13:31.
47. Bolotin DA, Poslavsky S, Mitrophanov I, Shugay M, Mamedov IZ, Putintseva EV, et al. MiXCR: software for comprehensive adaptive immunity profiling. *Nat Methods.* 2015;12(5):380-1.
48. Gu Z, Gu L, Eils R, Schlesner M, and Brors B. circlize Implements and enhances circular visualization in R. *Bioinformatics.* 2014;30(19):2811-2.

Main Figures

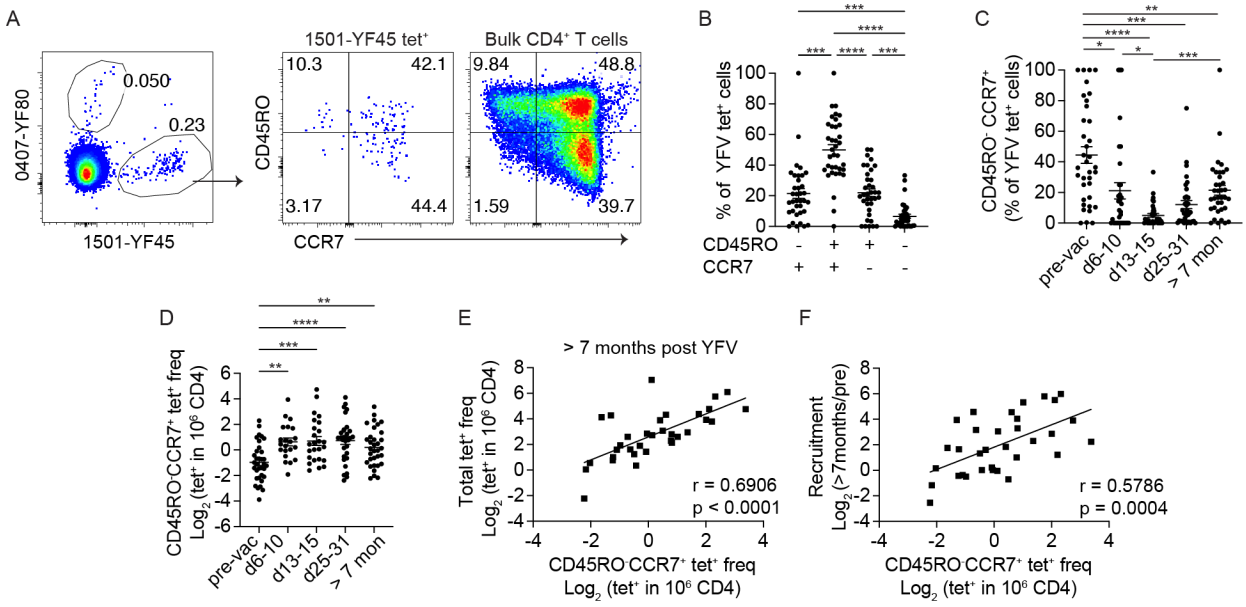

Figure 1: Identification of CD45RO$^-$CCR7$^+$ virus-specific CD4$^+$ T cells after YFV vaccination. (A) Direct *ex vivo* tetramer and antibody staining of a representative YFV tetramer$^+$ (tet$^+$) population using blood collected about 7 months after YFV vaccination. (B) The percentage of YFV tet$^+$ T cells with the indicated combination of CD45RO and CCR7 expression. Plot summarizes data from 36 specificities 7 to 34 months after YFV vaccination from 7 donors. (C-D) The abundance of CD45RO$^-$CCR7$^+$ YFV tet$^+$ CD4$^+$ T cells in 7 healthy subjects was quantified as a percentage of tetramer$^+$ cells (C) or by frequency (D). Each symbol represents data from a distinct YFV-specific population. Experiments were repeated an average of 3.3 times. (E) The correlation between CD45RO$^-$CCR7$^+$ YFV tet$^+$ T cell frequency and the overall tet$^+$ frequency of the same population at least 7 months after vaccination. (F) The correlation between the CD45RO$^-$CCR7$^+$ YFV tet$^+$ T cell frequency and the fold change from the pre-vaccine baseline to the memory time point. CD45RO$^-$CCR7$^+$ tet$^+$ frequencies were determined using samples taken 7 to 34 months after vaccination. n = 33, populations with no post-vaccine naïve cells were excluded. RM one-way ANOVA (B) or Mixed-effect analysis (C and D) was performed and corrected with Tukey's multiple comparisons test. For (E) and (F), Pearson correlation was computed.

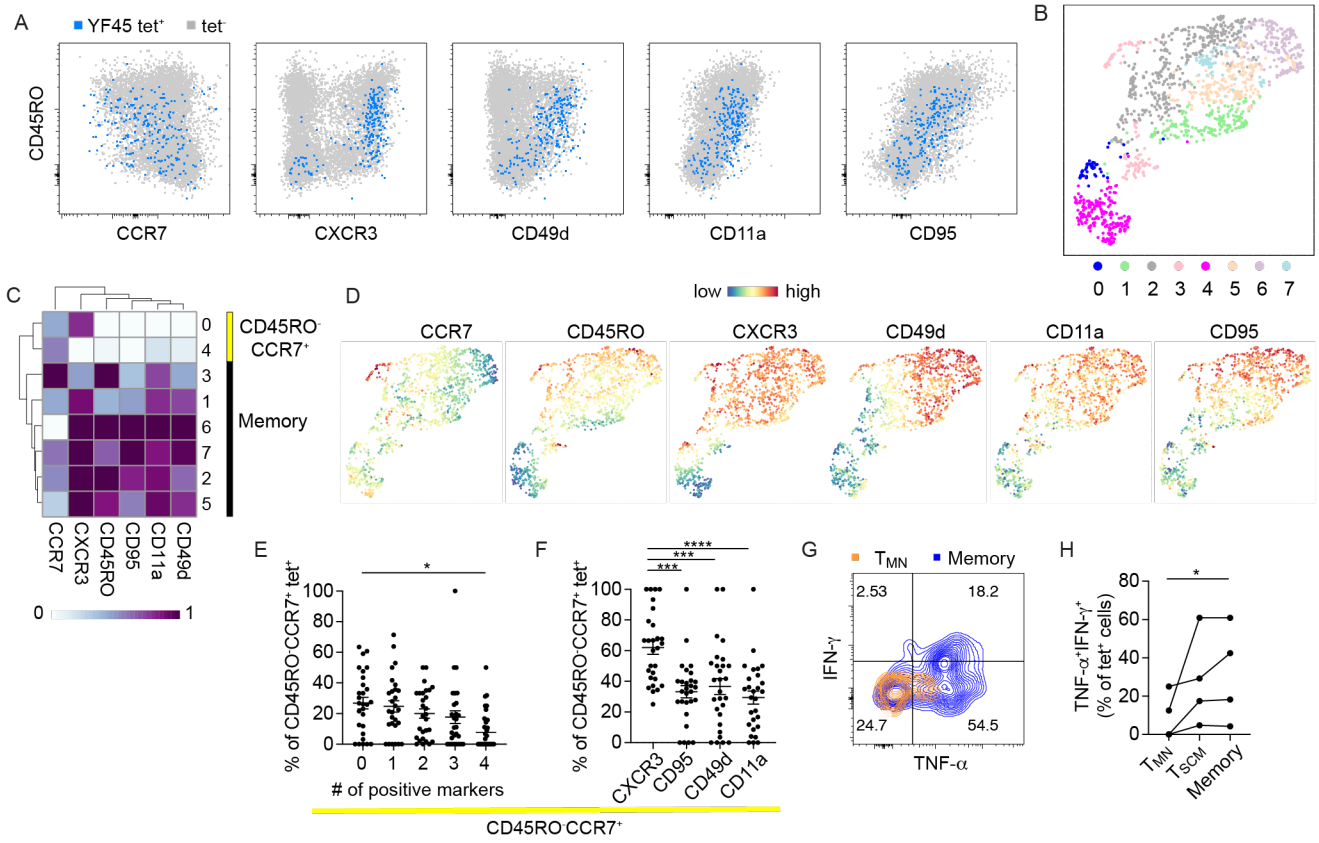

Figure 2: Post-vaccine CD4⁺ T cells are heterogeneous and include naïve-like subsets. (A) FACS plots show the expression of the indicated marker on a representative YFV-specific population. The tet⁺ population is overlaid onto tet⁻ bulk CD4⁺ T cells. (B) UMAP displays Phenograph-defined clusters. Data combine 1465 CD4⁺ cells labeled by 7 YFV tetramers from HD3. (C-D) The staining intensity of individual markers is shown on a heatmap for each cluster (C) or displayed on the UMAP. (E-F) The relative abundance of CD45RO⁻ CCR7⁺ YFV-specific T cells by the indicated numbers of markers (E) or the type of markers (F). Frequency in F combines all cells positive for a particular marker within the CD45RO⁻CCR7⁺ subset. Marker combinations were determined using Boolean operators on manually defined gates. Each symbol represents a tetramer⁺ population (n = 28). Experiments were repeated an average of 2.5 times. (G) PBMCs were stimulated for 4 - 5 hours by PMA and ionomycin and assayed for cytokine production by intracellular cytokine staining. The plot shows representative TNF-α and IFN-γ expression by T_{MN} cells and memory T cells (non-CD45RO⁻CD28⁺) from the same tetramer-labeled population. (H) T cell responses by TNF-α and IFN-γ production for the indicated phenotypic subset. Each population was identified with a pool of 5-7 tetramers of the same DR allele, using cells from 3 donors. For (E) and (F), RM one-way ANOVA was performed and corrected with Tukey's multiple comparison test. For (H), the Friedman test was performed and corrected using Dunn's multiple comparison test.

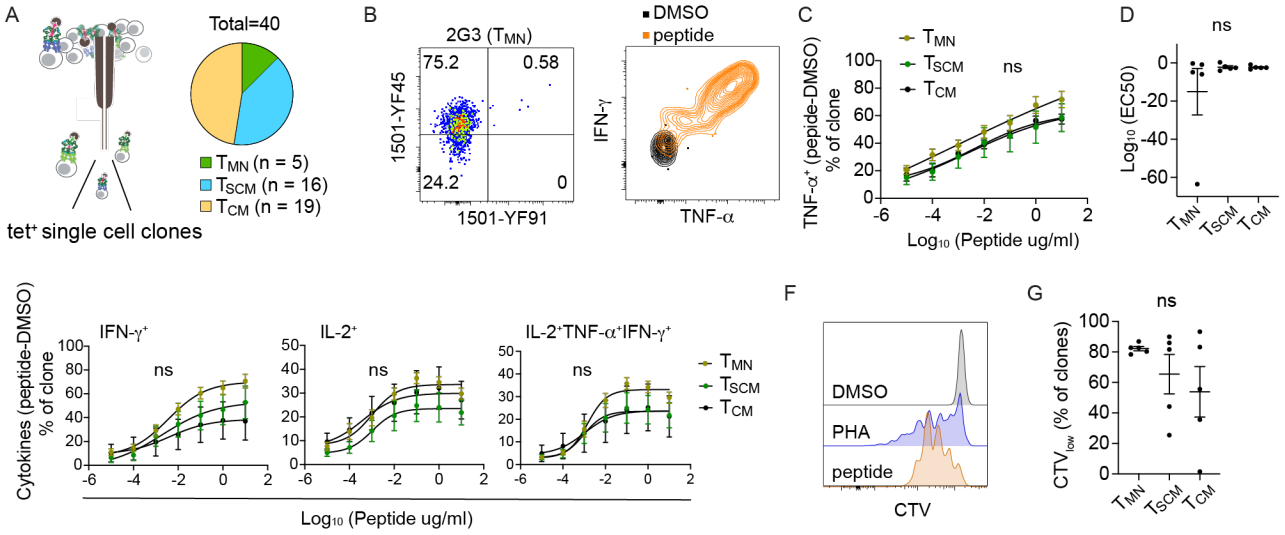

Figure 3: T_{MN}-derived T cell clones respond to antigen stimulation. (A) Schematics of single-cell T cell cloning. Post-vaccine T cells from HD2 and HD3 were stained with 1501-YF45 tetramers, sorted based on T_{MN}, T_{SCM}, or T_{CM} phenotypes, and expanded for 2 to 3 weeks in culture. (B) *In vitro* expanded T cell clones were re-stained with tetramers and cultured with vehicle or peptide-treated monocyte-derived dendritic cells. Representative plots show tetramer staining and cytokine production by intracellular cytokine staining. (C-D) T cell clones were stimulated with decreasing concentrations of YFV peptides. The response was measured by TNF-α production (C) and quantified by EC50 values after subtracting the background signal from vehicle-treated control (D). (E) Peptide dose response of T cell clones by IFN-γ, IL-2, and $IL2^{+}TNF\text{-}\alpha^{+}IFN\text{-}\gamma^{+}$ production. (F) Representative histograms show CTV dilution in response to 10ug/ml of peptide stimulation. (G) Plot summarizes the frequency of CTV_{low} population after a 5-day culture for clones in each phenotypic group. All experiments were repeated at least twice with n= 5 in each group. For (C) and (E), RM two-way ANOVA was performed and corrected with Tukey's multiple comparison test. For (D) and (G), Kruskal-Wallis test and Dunn's multiple comparison test were used.

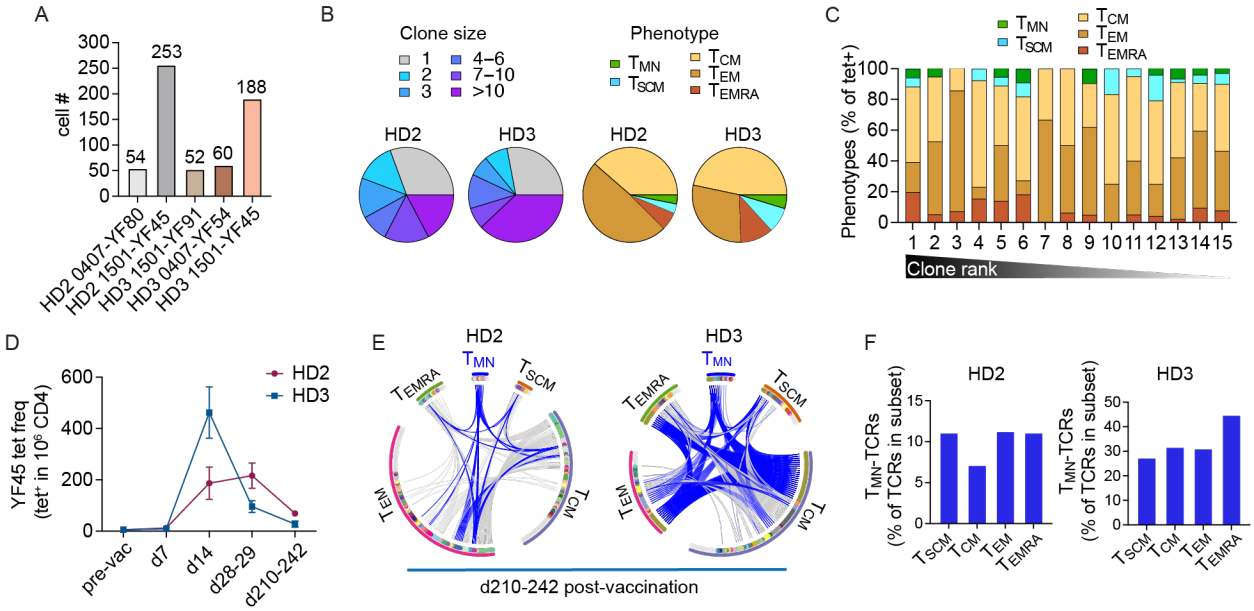

Figure 4: T_{MN} cells are clonally related to memory T cells. (A) The plot summarizes the number of cells sequenced from the indicated specificities and donors collected 242 (HD2) or 210 (HD3) days after primary YFV vaccination. (B) Clone size and phenotypic distribution of YFV tet$^+$ populations in A. Phenotypic information were obtained by index sorting. T_{MN} (CD45RO$^-$CCR7$^+$CXCR3$^-$CD95$^-$CD11a$^-$CD49d$^-$), T_{SCM} (CD45RO$^-$CCR7$^+$ and positive for at least one of CXCR3, CD95, CD11a, or CD49d), T_{CM} (CD45RO$^+$CCR7$^+$), T_{EM} (CD45RO$^+$CCR7$^-$), T_{EMRA} (CD45RO$^-$CCR7$^-$). Cells with ambiguous phenotypes were excluded. (C) Distribution of phenotypes in B by clonotype frequency, ranked from largest to unique clonotypes. (D) The frequencies of YF45-specific T cells pre-vaccine and at the indicated days following YFV immunization. (E) Each circus plot represents TCRs from YF45 tet$^+$ cells obtained 210-242 days after vaccination, separated by the associated indexed phenotypes. Cells are ordered by frequency within each arc. Gray marks cells expressing unique TCRs, other colors represent expanded or shared sequences. Shared TCRβ or TCRα and β, when a TCRα is available, is connected by a line across distinct phenotypic subsets. Blue lines highlight TCRs from T_{MN} cells that are shared with cells expressing other phenotypes. (F) The percentage of TCRs in each memory subset that matched T_{MN}-derived sequences.

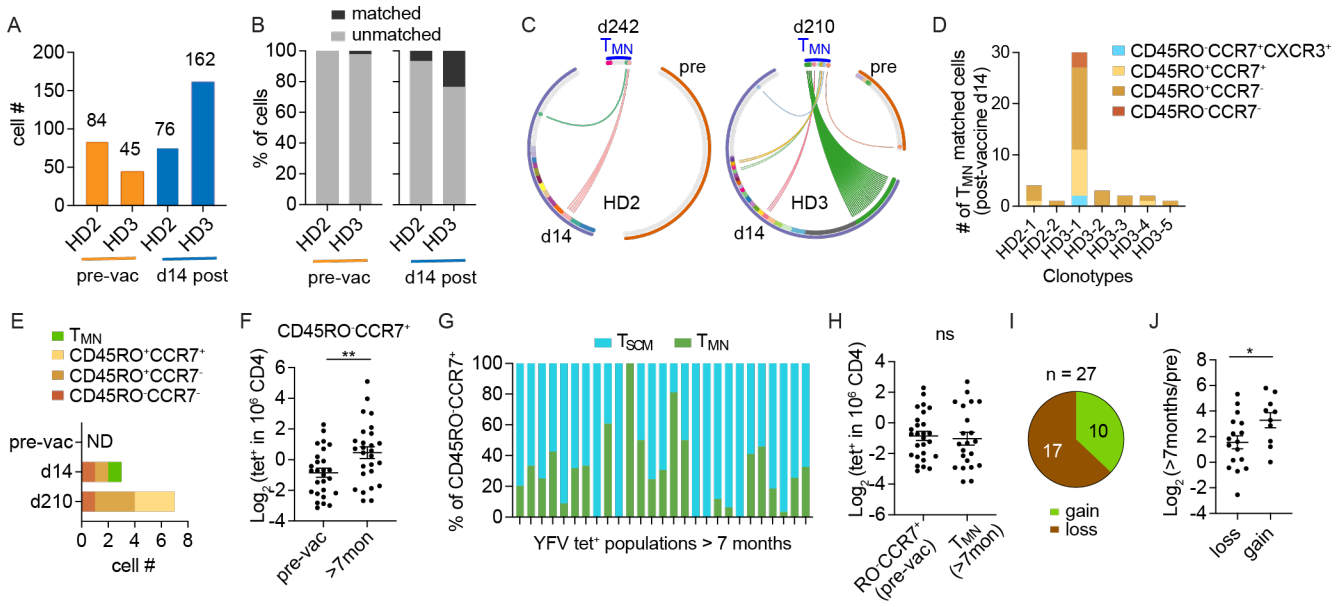

Figure 5: T_{MN} cells are clonally related to effector T cells and increased after vaccination. (A) The number of TCRs from YF45 tet$^+$ T cells from the indicated donors, before and 14 days after YFV vaccination. (B) TCRs from cells in A were compared to T_{MN}-derived TCRs in the day 210-242 post-vaccine samples. Bar-graphs show the percentages of cells with or without a match. (C) Each circus plot represents TCRs from T_{MN} YF45 tet$^+$ cells and TCRs from the same specificities, before and 14 days after YFV vaccination, from the same donors. Cells are ordered by frequency within each arc. Gray marks cells expressing unique TCRs, other colors represent expanded or shared sequences. Connecting lines highlight shared TCRs between a T_{MN} cell and cells in a previous time point. (D) The number and phenotypes of T cells in the day 14 sample that matched a T_{MN}-derived clonotype from the memory time point. (E) Clonal dynamics of a TCR expressed by a T_{MN} cell in the 14-day post-vaccine sample. Plot shows the number and phenotypes of T cells that expressed the same TCR sequence at the indicated time points. ND, not detected. (F-G) The frequencies of CD45RO$^-$CCR7$^+$ YFV-specific T cells before and after vaccination for the corresponding populations (F). Post-vaccine CD45RO$^-$CCR7$^+$ tet$^+$ cells were separated into T_{SCM} or T_{MN} subsets based on CXCR3, CD95, CD11a, or CD49d staining (G). (H) Plot compares the frequencies of CD45RO$^-$CCR7$^+$ tetramer$^+$ cells pre-vaccination with the frequencies of T_{MN} cells in the corresponding population from the post-vaccine sample. (I) The post-vaccine T_{MN} frequency of each tet$^+$ population was divided by its initial CD45RO$^-$CCR7$^+$ frequency before vaccination. The ratio is defined as a gain if above 1 and a loss if below 1. Pie chart shows the numbers of populations that had gained or lost naïve T cells after vaccination. (J) Plot shows the fold-change in tet$^+$ frequency, from the pre-vaccine baseline to the memory time point, for populations that had gained or lost naïve cells. For (F), (H), and (J), n = 27 tetramer$^+$ populations. Welch's t-test was performed.

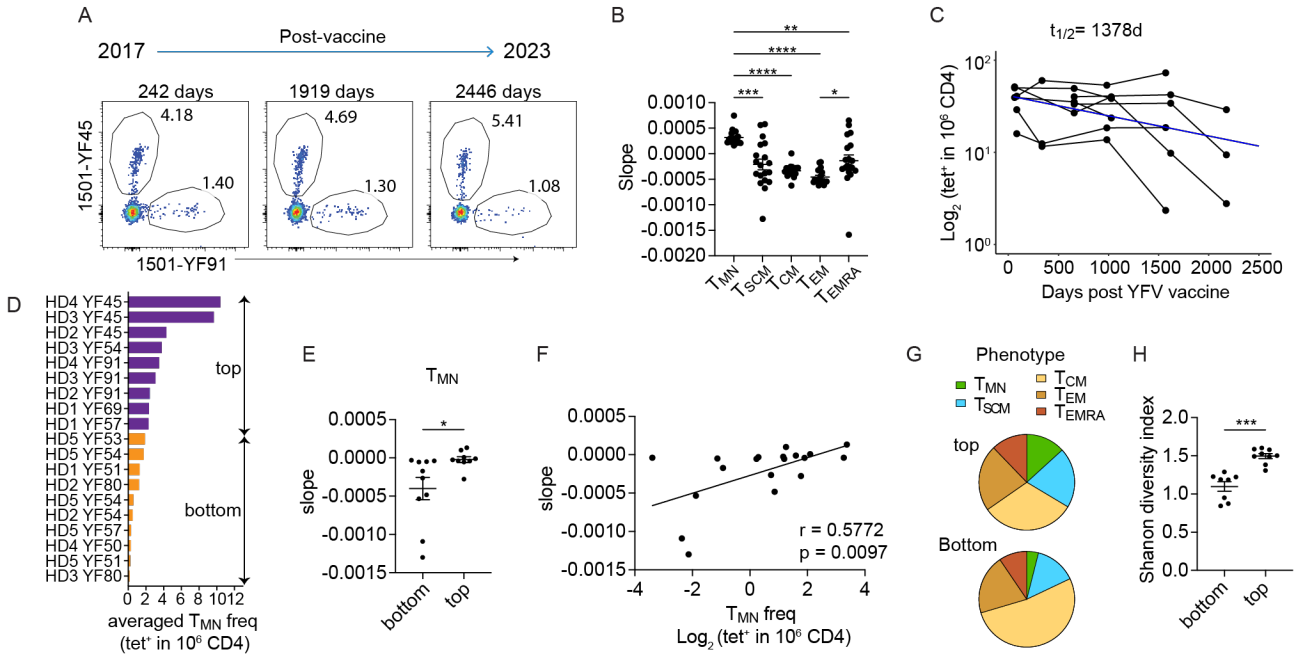

Figure 6: T_{MN} cells are stable and associated with durable T cell memory. (A) Representative plots show YFV-specific CD4$^+$ T cells over the indicated time points from HD2. (B) Each tet$^+$ population of a given specificity was subdivided according to phenotypes. The change over time for each phenotypic subset was quantified by the estimated slope using a mixed effects exponential decay model (n = 19 tetramer$^+$ populations from 5 donors). (C) A mixed effects exponential decay model fitted to the dynamics of YFV-specific CD4$^+$ T cells after a single YFV vaccination (n = 8 populations, combined from donors 4 and 5). The estimated decay (blue line) was used for calculating the half-life ($t_{1/2}$). (D) Ranking of tet$^+$ populations by the averaged frequency of T_{MN} cells within each population across all time points. (E) Plot summarizes the estimated slopes of individual tet$^+$ populations, divided into top and bottom halves by T_{MN} frequency in D. (F) The correlation between slopes characterizing the change over time for the overall tetramer$^+$ populations and their corresponding averaged T_{MN} frequencies. (G) Pie-charts show the distribution of memory subsets. Populations were divided into top and bottom groups by the first measured T_{MN} frequency obtained within 1-2 years after YFV vaccination. (H) Phenotypic diversity of each tet$^+$ population was quantified using Shannon Diversity Index, categorized into top or bottom groups based on T_{MN} frequency as in G. Each symbol represents one tetramer$^+$ population. Experiments were repeated an average of 2.3 times. Data are represented as mean ± SEM. For (B), RM one-way ANOVA was performed and corrected with Tukey's multiple comparisons test. Welch's t-test was performed for (E) and (H). For (F), Spearman correlation was performed.